



HAL
open science

A Simple Cloud Parameterization Derived from Cloud Resolving Model Data: Diagnostic and Prognostic Applications

Jean-Pierre Chaboureau, Peter Bechtold

► **To cite this version:**

Jean-Pierre Chaboureau, Peter Bechtold. A Simple Cloud Parameterization Derived from Cloud Resolving Model Data: Diagnostic and Prognostic Applications. *Journal of the Atmospheric Sciences*, 2002, 59 (15), pp.2362-2372. 10.1175/1520-0469(2002)0592.0.CO;2 . hal-04253280

HAL Id: hal-04253280

<https://hal.science/hal-04253280>

Submitted on 23 Oct 2023

HAL is a multi-disciplinary open access archive for the deposit and dissemination of scientific research documents, whether they are published or not. The documents may come from teaching and research institutions in France or abroad, or from public or private research centers.

L'archive ouverte pluridisciplinaire **HAL**, est destinée au dépôt et à la diffusion de documents scientifiques de niveau recherche, publiés ou non, émanant des établissements d'enseignement et de recherche français ou étrangers, des laboratoires publics ou privés.

Copyright

A Simple Cloud Parameterization Derived from Cloud Resolving Model Data: Diagnostic and Prognostic Applications

JEAN-PIERRE CHABOUREAU AND PETER BECHTOLD

Laboratoire d'Aerologie, Observatoire Midi-Pyrenees, Toulouse, France

(Manuscript received 17 July 2001, in final form 4 January 2002)

ABSTRACT

A simple statistical parameterization of cloud water-related variables that has been originally developed for nonprecipitating boundary layer clouds is extended for all cloud types including deep precipitating convection. Based on three-dimensional cloud resolving model (CRM) simulations of observed tropical maritime and continental midlatitude convective periods, expressions for the partial cloudiness and the cloud water content are derived, which are a function of the normalized saturation deficit Q_1 . It turns out that these relations are equivalent to boundary layer cloud relations described earlier, therefore allowing for a general description of subgrid-scale clouds.

The usefulness of the cloud relations is assessed by applying them diagnostically and prognostically in a mesoscale model for a midlatitude cyclone case and a subtropical case, and comparing the simulated cloud fields to satellite observations and to reference simulations with an explicit microphysical scheme. The comparison uses a model-to-satellite approach where synthetic radiances are computed from the meteorological fields and are compared to Meteosat satellite observations both in the visible and the thermal infrared spectral channels. The impact of the statistical cloud scheme is most pronounced for shallow and deep convective cloud fields (where $Q_1 < 0$), provided that the host models convection parameterization is able to correctly represent the ensemble average water vapor profile in the troposphere. The scheme significantly reduces the biases in the infrared and especially shortwave spectral range with respect to the explicit microphysical scheme. Furthermore, it produces more realistic (smooth) horizontal and vertical condensate distributions in both diagnostic or prognostic applications showing the potential use of this simple parameterization in larger-scale models.

1. Introduction

Clouds are among the most important regulators of the weather and climate of the earth's atmosphere. They are the product of complicated interactions between large-scale circulations, moist convective transport, small-scale turbulent mixing, radiation, and microphysical processes. Among the most important cloud systems of the climate system are tropical and subtropical shallow and deep convective cloud populations, midlatitudinal frontal clouds, stratocumulus cloud sheets over cold ocean water, and upper tropospheric cirrus clouds associated to upper-level jets or outflow from deep convective systems.

Clouds reflect the distribution of water vapor and temperature in the atmosphere (see, e.g., Zhang and Chou 1999 for tropical clouds), and therefore their representation in a meteorological model requires the knowledge of this distribution. Furthermore, due to the limited grid resolution of current numerical weather prediction

(NWP) models and general circulation models (GCMs), clouds appear as a subgrid-scale process, with cumulus clouds representing an essentially horizontal subgrid-scale process, and stratiform clouds representing a vertical subgrid-scale process. The representation of cloudiness and cloud condensate in GCMs is either diagnostic or prognostic (e.g., Smith 1990; Tiedtke 1993). Attention should also be given to the fact that current NWP models and GCMs generally use separate formulations for the large-scale (stratiform) transport/condensation and the convective transport/condensation of water vapor. Therefore, an additional difficulty arises in linking the convective cloudiness or moisture detrained from the convection scheme to the large-scale fields. When a diagnostic approach is used one can simply diagnose the cloudiness from the grid average (convectively adjusted) moisture and temperature fields. However, the prognostic approach requires two prognostic equations, one for the cloudy part and one for the clear-sky part of the grid (Tiedtke 1993), otherwise the cloud water detrained from the convection scheme would immediately evaporate; as in the presence of convection, the grid average moisture content is generally smaller than the saturation value.

Since the early theoretical work by Sommeria and

Corresponding author address: Dr. Jean-Pierre Chaboureau, Météo-France, CNRM/GMME/MOANA, 42 av. Coriolis, Toulouse 31057, France.
E-mail: jean-pierre.chaboureau@cnrm.meteo.fr

Deardorff (1977), Mellor (1977), and Bougeault (1981), many attempts have been made to formulate a subgrid-scale (fractional) cloudiness that can be applied to both stratiform and convective clouds. However, the verification of such schemes has been difficult and only increasing computer power made it possible to run three-dimensional large eddy simulation models (LESs) and cloud resolving models (CRMs) in order to evaluate the statistical properties of cloud fields. For example, statistical diagnostic parameterizations for cloudiness and cloud water content were developed by Cuijpers and Bechtold (1995, hereafter referred as to CB) based on LES data for nonprecipitating boundary layer clouds; whereas Cusack et al. (1999) used GCM simulations on different horizontal resolutions to determine the water vapor distribution. Diagnostic empirical approaches based on data from a two-dimensional CRM, proposed by Xu and Krueger (1991) and Xu and Randall (1996), use the relative humidity and the cumulus mass flux as a predictor.

The objective of the present paper is to extend the simple boundary layer cloud relations presented in CB to deep precipitating clouds and upper-level cirrus clouds using data from large-domain three-dimensional CRM simulations of observed tropical and midlatitude convective events. The manuscript is organized as follows. After a short presentation of the required thermodynamical framework, CRM data of deep convective events are used to deduce relations for the fractional cloudiness and the ensemble (grid) average cloud condensate content. Next, these expressions are applied in a mesoscale model for a midlatitude cyclone case and a subtropical case, and the impact of the scheme is assessed by a comparison with Meteosat satellite observations both in the visible and the thermal infrared spectral channels. Finally, some practical aspects of representing clouds in meteorological models and the validation methods using satellite data are discussed in the conclusions.

2. Thermodynamical framework

The properties of a moist adiabatically ascending air parcel are conveniently expressed assuming conservation (in the absence of precipitation) of enthalpy or “liquid water static energy” h_l [see Emanuel 1994, (4.5.25)] and total water mixing ratio r_w :

$$h_l = C_{pm}T - L_v r_c - L_s r_i + (1 + r_w)gz; \quad (1)$$

$$r_w = r_v + r_c + r_i, \quad (2)$$

where the specific heat of moist air is defined as $C_{pm} = C_{pd} + r_w C_{pv}$; L_v and L_s are the specific latent heats of vaporization and sublimation; g denotes the gravitational acceleration; z is height; and r_v , r_c , and r_i denote the mixing ratios of water vapor and nonprecipitating cloud water/ice, respectively. The definitions of the various thermodynamical constants and functions are pro-

vided in the appendix. We further define a “liquid” temperature as

$$\begin{aligned} T_l &= T - L_v/C_{pm}r_c - L_s/C_{pm}r_i \\ &= [h_l - (1 + r_w)gz]/C_{pm}, \end{aligned} \quad (3)$$

and combine the moisture and temperature effects to one single variable $s = ar_w - bT_l$ (see, e.g., Mellor 1977) with

$$\begin{aligned} a &= (1 + Lr_{sl}/C_{pm})^{-1}, \quad b = ar_{sl}, \\ r_{sl} &= \partial r_{\text{sat}}/\partial T(T = T_l) = Lr_{\text{sat}}(T_l)/(R_v T_l^2). \end{aligned} \quad (4)$$

Here L and r_{sat} are the latent heat and water vapor saturation mixing ratio that, inside a given glaciation interval $T_0 > T > T_1$, are linearly interpolated as a function of temperature between their respective values for liquid water and ice; that is, $L = (1 - \chi)L_v + \chi L_s$, $r_{\text{sat}} = (1 - \chi)r_{\text{satw}} + \chi r_{\text{sati}}$, with $\chi = (T_0 - T)/(T_0 - T_1)$, $T_0 = 273.16$ K, and $T_1 = 253$ K. Here, r_{satw} and r_{sati} are the saturation mixing ratios over water and ice, respectively.

Finally, with the above definitions, Q_1 is expressed as the saturation deficit of the ensemble or grid average (denoted by overbars) normalized by σ_s , the variance of s , with primes denoting deviations from the ensemble (grid) mean:

$$\begin{aligned} Q_1 &= \bar{a}[\bar{r}_w - r_{\text{sat}}(\bar{T}_l)]/\sigma_s, \\ \sigma_s &= [\bar{a}^2 \bar{r}_w'^2 - 2\bar{a} \bar{b} \bar{r}_w' \bar{T}_l' + \bar{b}^2 \bar{T}_l'^2]^{1/2}. \end{aligned} \quad (5)$$

However, an alternative expression for the normalized saturation deficit relating r_w to $r_{\text{sat}}(T)$ is also of interest:

$$\begin{aligned} Q_2 &= [\bar{r}_w - r_{\text{sat}}(\bar{T})]/\sigma_r, \\ \sigma_r &= [\bar{r}_w'^2 - 2\bar{r}_w' \bar{r}'_{\text{sat}}(\bar{T}) + \bar{r}'_{\text{sat}}(\bar{T})^2]^{1/2}. \end{aligned} \quad (6)$$

In the following, numerical data from CRM simulations of convective periods is used to empirically express the cloud fraction and the ensemble average condensate mixing ratio as a function of either Q_1 or Q_2 , avoiding any specification of probability distribution functions.

3. CRM study

a. Experiments and numerical setup

The use of numerical data from CRMs can now be considered a standard tool for evaluating and developing cloud parameterizations for GCMs (Moncrieff et al. 1997). The strategy consists in forcing CRMs with observed domain and time-averaged tendencies of temperature and water vapor, and in utilizing the ensemble CRM data as pseudo-observations of small-scale processes (Grabowski et al. 1996; Xu and Randall 1996; Wu et al. 1999; Guichard et al. 2000). In the present study the numerical data are obtained from the CRM version of the nonhydrostatic mesoscale model Méso-NH (Lafore et al. 1998) including in particular a 1.5-

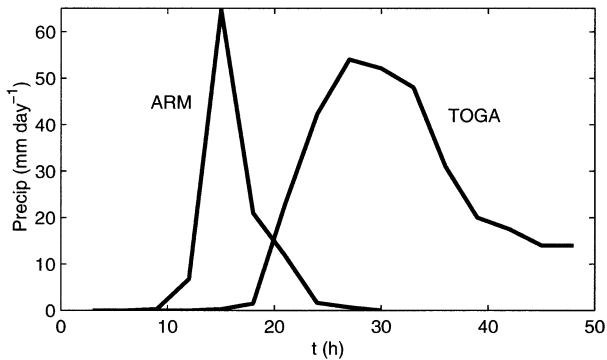


FIG. 1. Time evolution of simulated surface precipitation intensity (mm day^{-1}) for the ARM and TOGA COARE case.

order turbulence scheme, an interactive radiation parameterization and a prognostic microphysical scheme for five precipitating and nonprecipitating liquid and solid water categories. The model was run on a large domain including 256×256 horizontal grid points with a spacing of 2 km, and 47 vertical levels between the surface and the model top at 25 km; the model time step is 5 s. The case studies include (i) a tropical oceanic case observed during the Tropical Ocean Global Atmosphere Coupled Ocean-Atmosphere Response Experiment (TOGA COARE), that is, a 2-day period from 1200 UTC 10 December 1992 to 1200 UTC 12 December 1992 (Lin and Johnson 1996; Guichard et al. 2000), and (ii) a continental midlatitude convective case observed during the Atmospheric Radiation Measurement (ARM) experiment, that is, a 36-h period from 1200 UTC 29 June 1997 to 0000 UTC 1 July 1997 (Cederwall et al. 2000; Zhang et al. 2001). For each case study the model is forced with observed large-scale tendencies for temperature and moisture; however, the wind profile is relaxed toward observed values; for the ARM case the surface fluxes are also prescribed from observations. Boundary conditions are periodic. The model's initial conditions are horizontally uniform, but a small random temperature perturbation of 0.2 K is applied at the first model level in order to initiate convection.

The evolution of the domain-averaged surface precipitation as simulated by the CRM are depicted in Fig. 1. The ARM and TOGA COARE case studies include a strong convective period with maximum surface precipitation rates of 65 and 54 mm day^{-1} , respectively. In the following, cloud layer statistics are computed from 3-hourly snapshots of the simulations.

b. Fractional cloudiness and cloud condensate

The CRM-derived cloud fraction N and the normalized cloud condensate content r_l/σ_s are displayed in Figs. 2a,b as a function of Q_1 (the data came from all model levels). Here, N is defined at every vertical model level as the number of grid points with $r_l = r_c + r_i > 0$ divided by the total number of horizontal grid points.

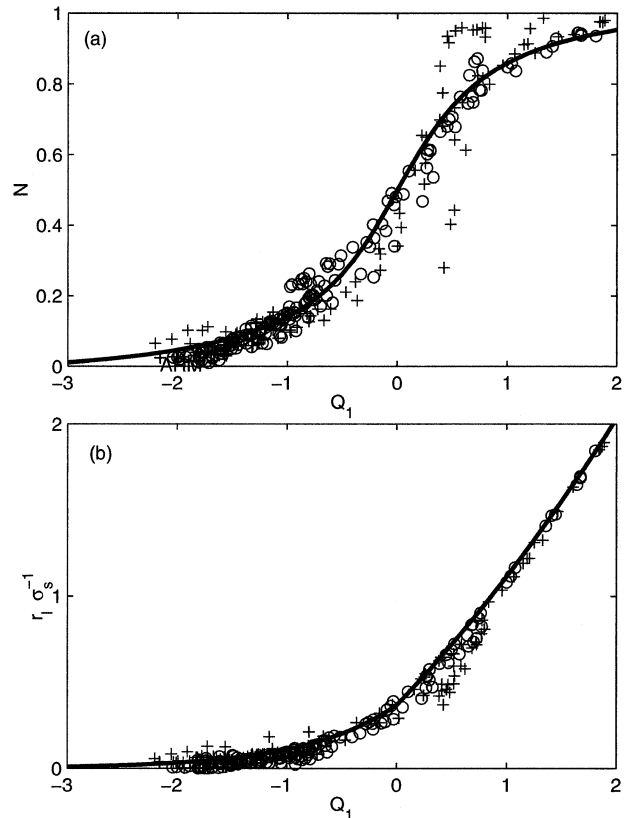


FIG. 2. Cloud fraction (a) and normalized condensate content (b) as a function of Q_1 . The experimental points are CRM results taken at different instances of the ARM (circles) and TOGA COARE (crosses) simulations, respectively. The solid lines correspond to the analytical functions given in CB.

The corresponding analytical cloud relations as suggested by CB are also illustrated in Fig. 2, where

$$N = \max\{0, \min[1, 0.5 + 0.36 \arctan(1.55Q_1)]\}, \quad (7)$$

$$\frac{\bar{r}_l}{\sigma_s} = e^{(1.2Q_1-1)}, \quad Q_1 < 0,$$

$$\frac{\bar{r}_l}{\sigma_s} = e^{-1} + 0.66Q_1 + 0.086Q_1^2 \quad 0 \leq Q_1 \leq 2,$$

$$\frac{\bar{r}_l}{\sigma_s} = Q_1, \quad Q_1 > 2. \quad (8)$$

Interestingly, the analytical results derived for boundary layer clouds also fit the present CRM results for deep precipitating convective situations, suggesting a broad application of these relations. Note that, in the definitions (1)–(2), the precipitating species are not included, otherwise the cloud relations (7)–(8) are not satisfied (not shown). The results for $Q_1 > -1$ are close to the Gaussian cloud relations discussed in Mellor (1977). The spread in the CRM results for TOGA COARE for positive values of Q_1 (i.e., the ensemble average values are oversaturated) is attributed to the

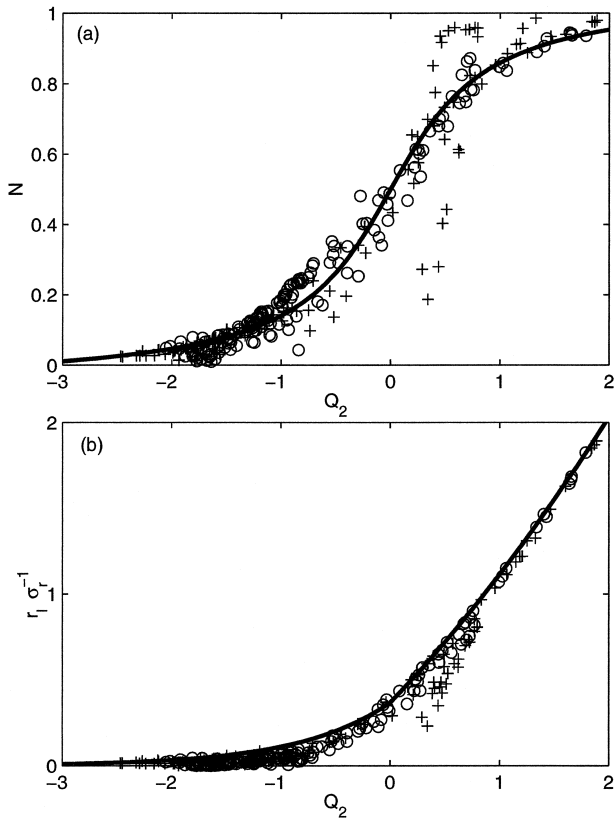


FIG. 3. As in Fig. 2, but as a function of Q_2 .

insufficient statistical representation of upper-tropospheric cirrus clouds due to the relatively low vertical model resolution of 700 m above the 12-km level.

Next, the possibility of using Q_2 [see (6)] instead of Q_1 is checked in Fig. 3. The results are similar to that

discussed in Fig. 2, especially for N . However, concerning the normalized condensate content a more rapid decrease to zero is observed for $Q_2 < 0$. Therefore, for actual model applications one would prefer using (7)–(8) as a function of Q_1 , however the fractional cloudiness can be reasonably represented using either Q_1 or Q_2 .

c. Parameterization of σ_s

The practical application of the cloud relations (7) and (8) in meteorological models requires the knowledge of the second-order moment σ_s . Here, a simple parameterization is suggested based on first-order turbulence closure and the stationarity assumption of the second-order moments:

$$\sigma_s = c_\sigma l \left[\bar{a}^2 \left(\frac{\partial \bar{r}_w}{\partial z} \right)^2 - 2\bar{a}\bar{b}C_{pm}^{-1} \frac{\partial \bar{h}_1}{\partial z} \frac{\partial \bar{r}_w}{\partial z} + \bar{b}^2 C_{pm}^{-2} \left(\frac{\partial \bar{h}_1}{\partial z} \right)^2 \right]^{1/2}, \tag{9}$$

where $C_{pm}^{-1} \partial h_1 / \partial z = \partial T_l / \partial z + g / C_{pm} (1 + r_w)$, l is a length scale, and c_σ is a constant of value 0.2 (Cuxart et al. 2000). Equation (9) only includes quantities that are known in any model. However, an alternative formulation based on the convective mass flux might be obtained following Lenderink and Siebesma (2000). The time-averaged vertical profiles and respective standard deviations of σ_s for the TOGA and ARM experiments are displayed in Fig. 4. All profiles exhibit a quasi-monotonic decrease of σ_s with height between the top of the boundary layer (located at $z = 500$ m for TOGA and at 1500 m for ARM) and the tropopause level; a typical order of magnitude for σ_s is 4×10^{-4} (see also CB). The larger time variability for ARM is associated with the passage of a midlatitude disturbance. Further-

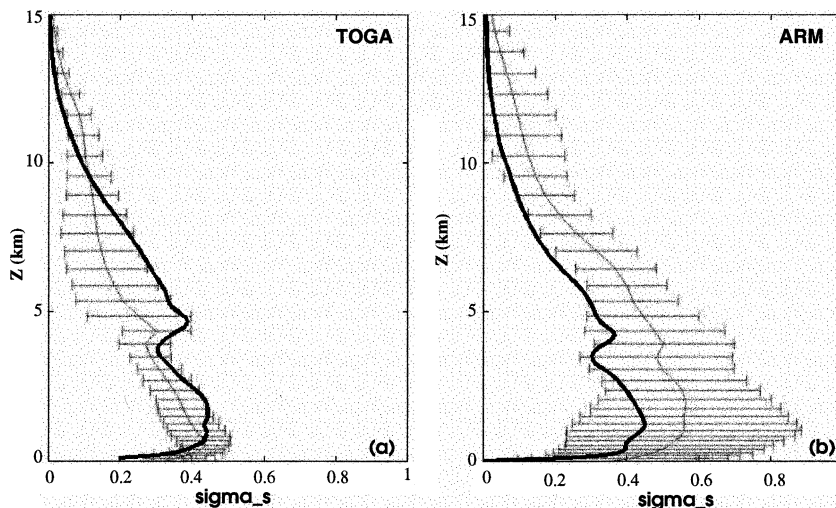


FIG. 4. Time-averaged vertical profiles of σ_s and their standard deviation for the (a) TOGA COARE and (b) ARM experiments as simulated by the CRM (thin solid lines) and parameterized with the aid of (9) (thick solid lines). Values of σ_s in the x axis are divided by 10^{-4} .

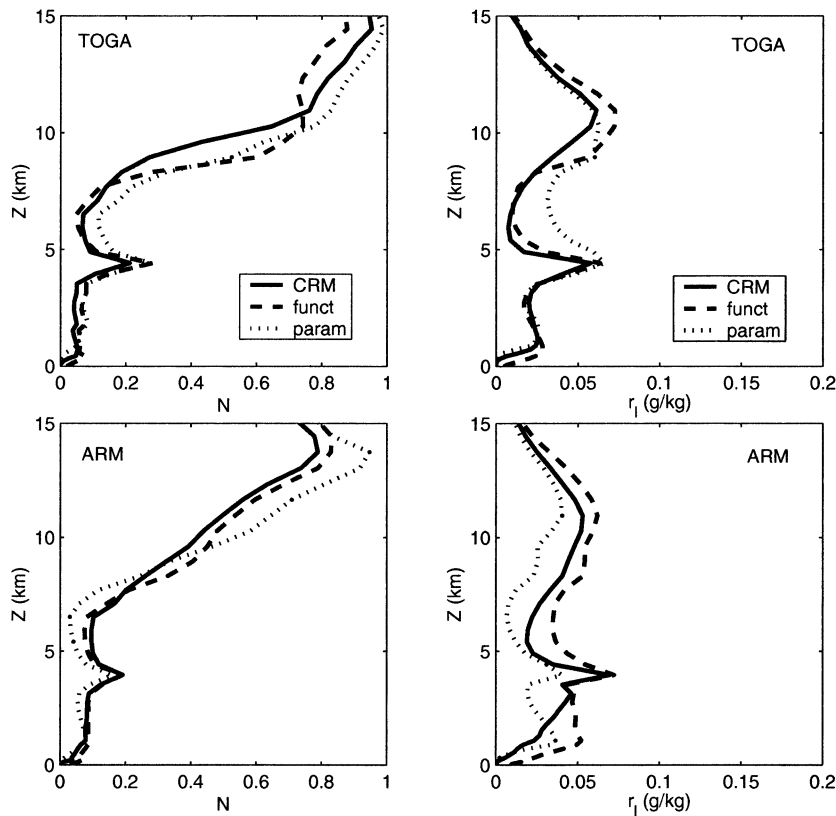


FIG. 5. Time-averaged vertical profiles of cloud fraction N and condensate mixing r_1 for TOGA and ARM: CRM results (solid lines), using relations (7)–(8) after CRM derived values of σ_s (dashed lines), using relations (7)–(8) together with parameterized values of σ_s following (9) (dotted lines).

more, the small discontinuity in the σ_s profiles corresponds to the 0°C isotherm, but might be exaggerated by the model's microphysical scheme. The parameterized profiles are also plotted in Fig. 4, using a constant free tropospheric length scale $l = 900$ m, a value that has been determined experimentally as the best fit of (9) to the CRM results. Inside the boundary layer ($z < l$), l is simply set equal to z , the height of the model layer, but more sophisticated formulations might be more appropriate (e.g., Bougeault and Lacarrère 1989; Holtslag and Nieuwstadt 1986). The results show that (9) gives a reasonable approximation of σ_s provided that the variances are computed from gradients of conserved variables.

Finally, the usefulness of the cloud parameterization is checked by comparing in Fig. 5 the time-averaged vertical profiles of the cloud fraction and the condensate mixing ratio obtained from the CRM to the corresponding profiles obtained using (i) the cloud relations (7)–(8) together with the CRM derived values of σ_s , and (ii) the cloud relations (7)–(8) together with the parameterized values of σ_s using (9). The results show that the parameterization closely reproduces the cloud fraction profiles for both the TOGA COARE and ARM case. However, the condensate profiles are more sensitive to

the choice of σ_s . The parameterization slightly overestimates the cloud condensate for TOGA and underestimates the values for ARM, indicating that the length scale l in (9) might vary as a function of stability.

4. Mesoscale simulations and comparison with satellite observations

a. Mesoscale simulations

In the following, the cloud parameterization is applied in a mesoscale model and its impact is evaluated based on model simulations of midlatitude and subtropical cloud systems, and subsequent comparisons with satellite observations. The model is the nonhydrostatic mesoscale model Méso-NH, previously described. The free tropospheric vertical grid length is set to 700 m for the midlatitude case and 300 m for the subtropical case. Horizontal grid lengths are 40 and 30 km, respectively. Therefore the model includes a parameterization for shallow and deep subgrid-scale convective transport and precipitation (Bechtold et al. 2001).

The midlatitude case is from the Fronts and Atlantic Storm-Track Experiment (FASTEX) intensive observing period 16 (IOP16). The simulation covers $6480 \times$

4800 km over the North Atlantic Ocean, is initialized by Météo France/ARPEGE reanalyses at 0000 UTC 17 February 1997, and is integrated forward for 12 h. The subtropical case is taken from the PICO3 (subtropical ozone peaks) experiment. The PICO3 simulation covers 5400×5400 km in the subtropical North Atlantic sector. It is also integrated for 12 h starting with European Centre for Medium-Range Weather Forecasts (ECMWF) analyses at 1200 UTC 20 October 2000. The fields included in the initial and boundary conditions of the numerical experiments are only temperature, winds, and water vapor. No cloud initialization of the numerical experiments is performed; that is, the mixing ratio of the liquid and ice water species build themselves during the course of the simulations.

For the two control simulations (CTRL), the cloud scheme is the explicit five-categories microphysical parameterization already used for the CRM simulations. For both the midlatitude and subtropical cases the statistical cloud scheme is applied diagnostically to the fields predicted by the corresponding CTRL simulation after 12 h. However, for the subtropical case an additional simulation (PROG) is run using the statistical cloud scheme in prognostic mode. A prognostic application of the scheme is achieved by replacing the condensation/evaporation tendencies in the prognostic equations for r_c , r_i , r_v , and T by the following tendencies

$$\begin{aligned} \left. \frac{\partial \bar{r}_c}{\partial t} \right|_{\text{cond/evap}} &= \frac{[(1 - \chi)\bar{r}_i - \bar{r}_c^*]}{\Delta t}, \\ \left. \frac{\partial \bar{r}_i}{\partial t} \right|_{\text{cond/evap}} &= \frac{[\chi\bar{r}_i - \bar{r}_i^*]}{\Delta t}, \\ \left. \frac{\partial \bar{r}_v}{\partial t} \right|_{\text{cond/evap}} &= -\left. \frac{\partial \bar{r}_c}{\partial t} \right|_{\text{cond/evap}} - \left. \frac{\partial \bar{r}_i}{\partial t} \right|_{\text{cond/evap}}, \\ \left. \frac{\partial \bar{T}}{\partial t} \right|_{\text{cond/evap}} &= \frac{L_v}{C_{pm}} \left. \frac{\partial \bar{r}_c}{\partial t} \right|_{\text{cond/evap}} + \frac{L_s}{C_{pm}} \left. \frac{\partial \bar{r}_i}{\partial t} \right|_{\text{cond/evap}}, \quad (10) \end{aligned}$$

where \bar{r}_i is diagnosed from (8), χ is the fraction of liquid and solid condensate defined previously, Δt is the model time step, and the asterisks denote values at the previous time step.

b. Synthetic observations

Synthetic radiances corresponding to the Meteosat IR channel, in the thermal infrared window (10.5–12.5 μm), were computed by the narrowband radiative transfer code designed by Morcrette and Fouquart (1985) with 10 spectral bands as described in Chaboureau et al. (2000, 2002). Radiances are then converted to brightness temperatures (BTs), taking into account the filter function of the IR channel. The cloud radiative properties for liquid water are parameterized following Stephens (1978), whereas the radiative properties for cloud

ice are based upon Kristjánsson et al. (1999). The maximum-random cloud overlap assumption is assumed.

Synthetic radiances corresponding to the Meteosat visible (VIS) channel, were computed by the large-band radiative transfer code designed by Fouquart and Bonnel (1980) and used by the model to compute the shortwave radiative tendencies. The cloud optical properties are derived from Fouquart (1987) for the cloud water droplets, and from Ebert and Curry (1992) for the cloud ice crystals. This large-band code has been roughly modified to take into account the viewing angle of the satellite. However, the resulting synthetic radiances are sufficiently realistic to be compared with the observations.

In the next subsections, synthetic observations are labeled (i) *explicit* when obtained from the CTRL simulation using the cloud condensates determined by the explicit microphysical cloud scheme, (ii) *diagnostic* when obtained from the CTRL simulation using the cloud condensates diagnosed by the statistical cloud parameterization, and (iii) *prognostic* when obtained from the PROG simulation. Biases between model and observation are also given for either infrared BTs or visible radiances. They are obtained by averaging the differences between simulated and observed radiative quantities over the domains shown in Figs. 6 and 7.

c. Midlatitude case

Figure 6 shows the results of the model-to-satellite approach applied to the midlatitude case at 1200 UTC 17 February 1997, both in the VIS and the IR Meteosat channels. Only the southeastern part of the simulation domain, most illuminated by the sun, is displayed. Several synoptic cloud features, with radiances larger than $60 \text{ W m}^{-2} \text{ sr}^{-1}$ can be observed on the Meteosat images (Figs. 6a,b). First, the cloud system of IOP16 over the British Isles, with BTs less than 255 K, is characterized by a warm front ahead, a cloud head to the northwest of Ireland, and a trailing cold front. Second, the cirriform cloud pattern lying along 45°N between 40° and 20°W , which is associated with the jet stream and the warm front of a secondary low, displays low BTs of less than 235 K and moderate radiances, between 60 and $70 \text{ W m}^{-2} \text{ sr}^{-1}$. Third, the convective cloud fields located in the rear of the Irish low (north of 45°N) and off the Portuguese coast (between 20° and 10°W) are clearly distinct in the visible image (Fig. 6b). These cumulus clouds that developed in convectively unstable areas exhibit moderate BTs between 245 and 275 K.

These synoptic key patterns are also present at the same locations in the two synthetic BT images (Figs. 6c,e) with or without the use of the subgrid-scale cloud parameterization. Indeed, as these cloud systems are largely a result of the dynamical forcing, the good agreement found in the location and the BT intensity of the cloud systems between the observed and explicit IR BTs reflects the quality of the dynamical fields in the Mésoscale simulation. The subgrid-scale cloud parameteriza-

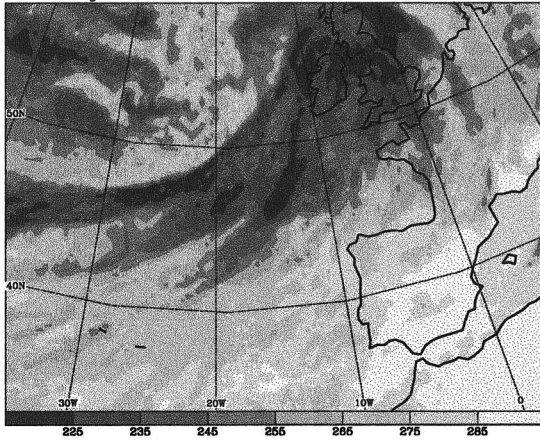
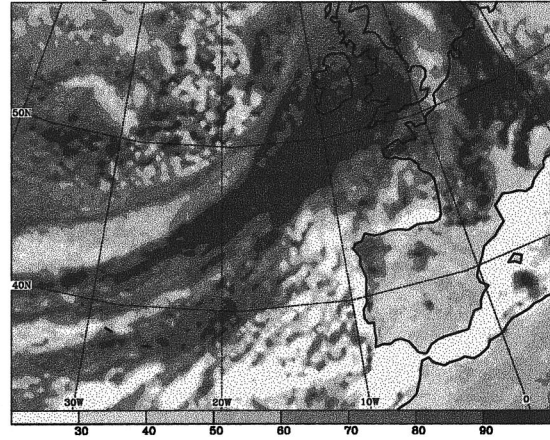
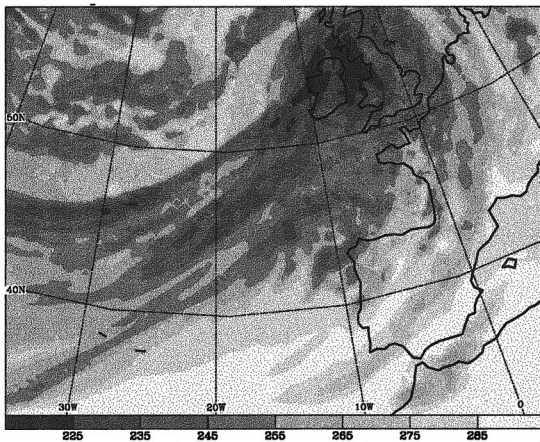
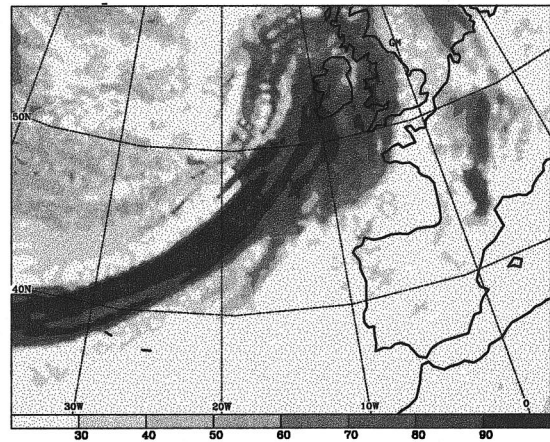
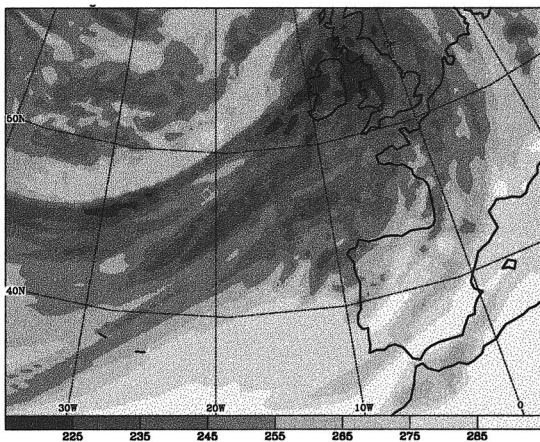
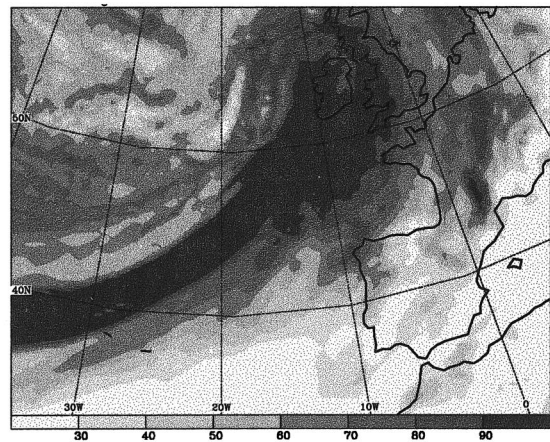
(a) observed IR BT**(b) observed VIS radiance****(c) explicit synthetic IR BT****(d) explicit synthetic VIS radiance****(e) diagnostic synthetic IR BT****(f) diagnostic synthetic VIS radiance**

FIG. 6. Midlatitude case at 1200 UTC 17 Feb 1997: IR BT (K) and VIS radiances ($\text{W m}^{-2} \text{sr}^{-1}$) obtained respectively from (a),(b) observation, and from CTRL simulation using the cloud condensates, (c),(d) produced by the explicit microphysical cloud scheme, and (e),(f) diagnosed by the cloud parameterization.

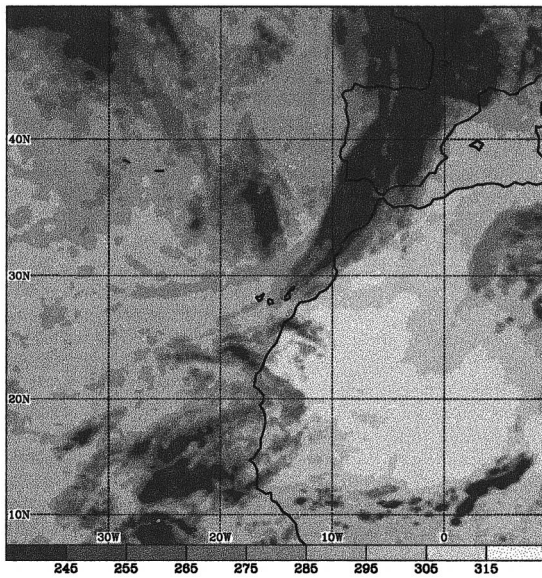
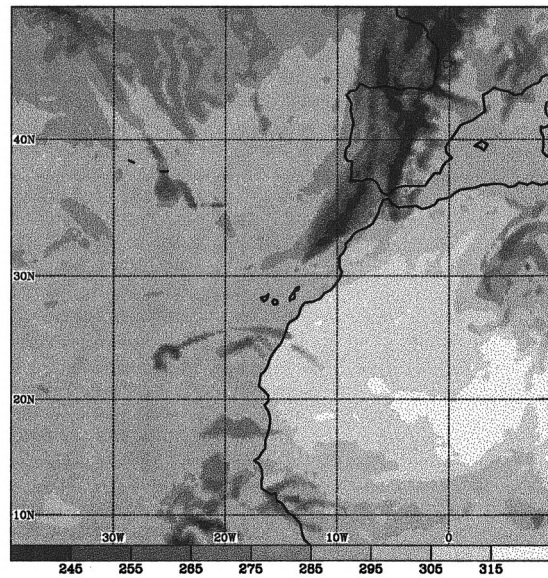
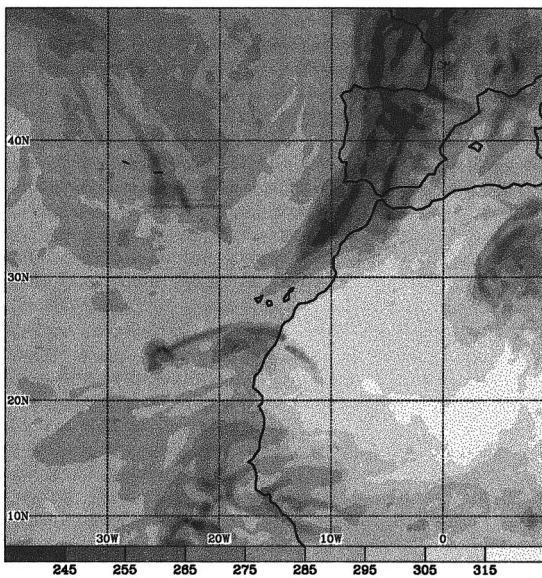
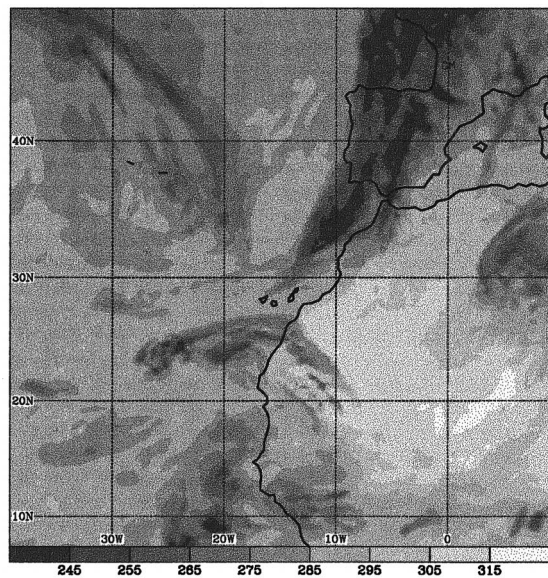
(a) observed IR BT**(b) explicit synthetic IR BT****(c) diagnostic synthetic IR BT****(d) prognostic synthetic IR BT**

FIG. 7. Subtropical case at 1200 UTC 20 Oct 2000: IR BTs (K) obtained from (a) observation, from the CTRL simulation using the cloud condensates, (b) produced by the explicit microphysical cloud scheme, (c) diagnosed by the statistical cloud parameterization, and (d) from the PROG simulation using the statistical cloud parameterization in a prognostic way.

tion is able to correctly diagnose the condensate mixing ratios at the stratiform cloud tops and slightly improves the representation of BTs in the convective cloud fields. Thus, the domain-averaged bias is reduced to -0.9 K compared to 2.0 K for the explicit experiment.

But the effect of the cloud parameterization has a much larger impact in the visible spectral range where the presence of reflectors such as clouds dramatically modifies the radiances observed from space. In the ex-

PLICIT VIS image (Fig. 6d) only the frontal areas of the cloud system of IOP16 display radiances over 60 $W m^{-2} sr^{-1}$. These large values are also present at the same location in the observed and diagnostic images (Figs. 6b,f). But outside these ascending frontal areas, the explicit VIS image exhibits low radiances of less than 50 $W m^{-2} sr^{-1}$, where large values are observed. This results in a domain-averaged bias of -24 $W m^{-2} sr^{-1}$. This default in representing optically thick clouds is

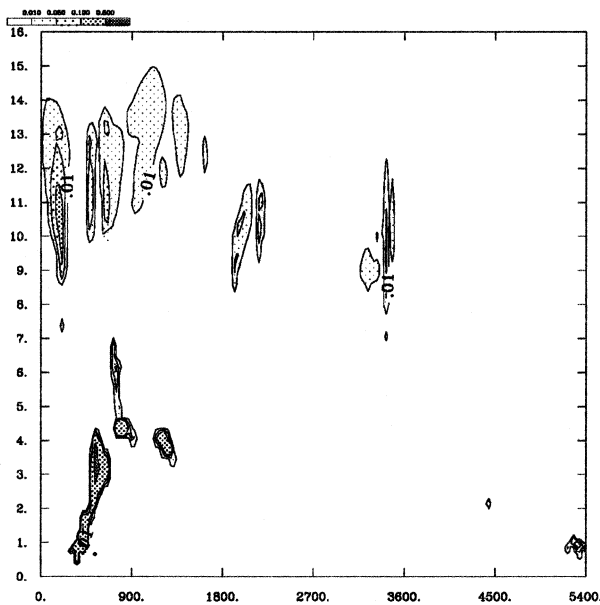
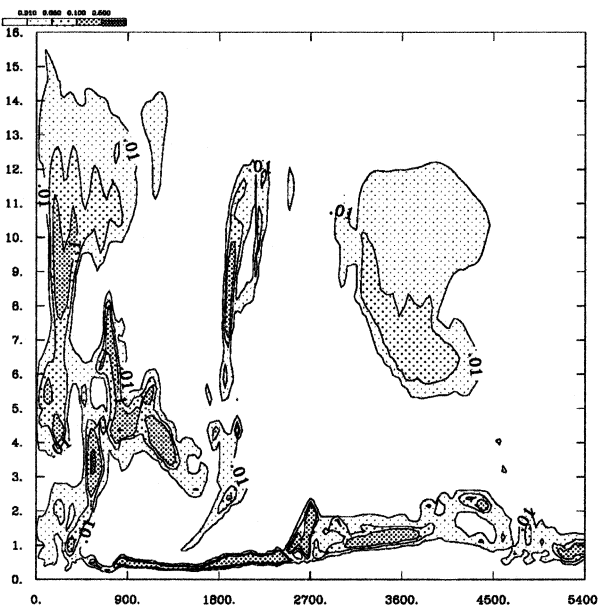
(a) CTRL simulation**(b) PROG simulation**

FIG. 8. Subtropical case at 1200 UTC 20 Oct 2000: Vertical cross section between 7°N , 20°W , left-hand side, and 48°N , 20°W , right-hand side, of nonprecipitating ice and cloud liquid mixing ratios from (a) the CTRL and (b) the PROG simulations. Figures on axis represent distance in kilometers. The solid lines are contours representing 0.01, 0.05, 0.1, and 0.5 g kg^{-1} .

corrected by the use of the cloud parameterization and its ability to realistically diagnose subgrid-scale condensate over the whole tropospheric column (see discussion in the next subsection). Thus, the diagnostic VIS image shows a larger spatial cloud signature in the as-

ending stratiform frontal areas but also in the jet stream region. This results in a better overall agreement with the observations, with a bias that is reduced to $-4 \text{ W m}^{-2} \text{ sr}^{-1}$. Another improvement given by the cloud parameterization can be seen in the cumulus cloud areas, where the radiances are increased to values above $30 \text{ W m}^{-2} \text{ sr}^{-1}$. However, the spatial variability of the broken clouds as observed in the VIS channel is underestimated by the cloud parameterization, which gives more uniform radiances.

To summarize, the use of the cloud parameterization in calculating synthetic observations leads to a better agreement with the Meteosat images, particularly in broken cloud areas both in the VIS and IR channels, and also in the stratiform frontal zones when looking at the VIS channel.

d. Subtropical case

The results for the subtropical Atlantic case are shown in Fig. 7. The displayed snapshot corresponds to 1200 UTC, after 12 h of simulation. Low observed BTs, less than 255 K, are associated with a frontal system extending from France to the north of the Canary Islands, and with deep convective systems over the ocean south of 25°N and over Algeria (Fig. 7a). Medium BTs around 270 K correspond to a midlatitude cloud system entering the northwestern part of the domain. The cold sector in the rear of the front over western Europe is characterized by cumulus cloud fields with BTs between 275 and 285 K.

In the resulting explicit IR image, the main cloud systems appear at the right location revealing the quality of the simulated dynamical fields (Fig. 7b). However, the cloud patterns generally have a smaller spatial extent with larger BT than the observed ones. Moreover, large oceanic areas of high and homogeneous BTs appear to be typical for clear sky in the explicit simulation, whereas broken cloud fields are observed at the same locations. These discrepancies result in a domain-averaged bias of 11 K.

The differences between the observation and the CTRL simulation are significantly reduced with the aid of the cloud parameterization, as shown by the diagnostic synthetic IR image (Fig. 7c). As already seen for the midlatitude case, the areas with BTs less than 255 K exhibit a larger spatial extent than in the explicit IR image, in particular the frontal system over Western Europe, the northwestern cloud system, and the oceanic and African deep convective systems. Furthermore, shallow and deep convective cloud systems now appear in the North Atlantic cold sector and over parts of the tropical and subtropical ocean. With the aid of the diagnostic cloud parameterization, the domain averaged bias is reduced to 7 K.

Finally, the prognostic synthetic IR image obtained from the PROG simulation (Fig. 7d) is similar to the synthetic IR image diagnosed from the CTRL simulation,

in spite of the fact that the modified cloud field now interacts with the dynamics and thermodynamics of the model. Furthermore, the PROG simulation produces an overall smoother cloud field, (avoiding, for example, the unphysical oscillations near 40°N, 25°W in Figs. 7b,c) and more realistically represents the cold frontal band and the southeasterly propagating cloud field in the northwestern part of the domain. As a consequence, the domain-averaged bias is further reduced to 5 K.

The vertical structure of the simulated cloud fields is examined with the aid of a vertical cross-section along 20°W from 7° to 48°N across the tropical deep convective cloud systems, the trailing cold front, and the post-frontal shallow convective region (Fig. 8). The CTRL simulation represents the tropical convective system (located between 0 and 900 km) by a lower and upper tropospheric cloud layer (Fig. 8a). In contrast, the PROG simulation produces a more homogeneous vertical structure of the convective cloud systems (represented by the sum of the liquid+ice condensate mixing ratios) with cloud bases at 500 m and cloud tops that attain 15 km. Furthermore, the PROG simulation produces a second deep convective system at 1800 km and a shallow convective cloud field north of the cold frontal band located at 2700 km. All these features are missing in the CTRL simulation. However, it is possible that the PROG simulation overestimates the subtropical low-level cloud fields between 900 and 2500 km due to the simple mixing formulation in (9).

5. Summary and conclusions

With the aid of numerical data from three-dimensional CRM simulations of tropical maritime and continental midlatitude precipitating convection, relations for the fractional cloudiness and the ensemble average condensate content have been determined that are a function of the normalized saturation deficit only.¹

It is shown that these relations are equivalent to the boundary layer cloud relations proposed by CB, therefore allowing for a general description of cloudiness. However, the cloud relations require the knowledge of second-order moments for temperature and moisture that must be parameterized in large-scale meteorological models. A simple parameterization based on first-order turbulent closure is suggested that gives a reasonable estimate of the variances in the free troposphere when a constant mixing length of 900 m is used.

The cloud parameterization has been applied as a diagnostic scheme in a mesoscale model for (i) a North Atlantic cyclone case with frontal cloud systems and widespread postfrontal deep and shallow convective cloud fields and (ii) as a diagnostic and prognostic scheme for cloud systems over the subtropical Atlantic.

Synthetic radiances were computed from the meteorological fields (i.e., predicted profiles of temperature, water vapor, and stratiform cloud condensate, as well as diagnosed fractional cloudiness and condensate profiles in the convective model columns) that allowed detailed comparisons with Meteosat satellite observations in both the visible and the thermal infrared spectral channels. The model results necessarily depend on the initial moisture analysis. However, they also strongly depend on the convection scheme, and particularly the ability of the convection scheme to represent the temporal and spatial distribution of convection, and to correctly represent the grid-average total water-temperature profiles as well as the correct cloud-top heights.

The most dramatic effect of the cloud parameterization is to minimize the domain-averaged difference between synthetic and observed images, from 25 to 4 $W m^{-2} sr^{-1}$ for the midlatitude VIS radiances and from 11 to 5 K for the subtropical IR BTs. The scheme exhibits significant improvement with respect to the control simulation with an explicit microphysical scheme for both stratiform and convective clouds. Furthermore, it produces smoother horizontal and vertical distributions of clouds, a feature that might be also important for the numerical stability of the host model.

Finally, concerning practical applications of present parameterizations in meteorological models, it is suggested to apply this parameterization either diagnostically or prognostically for both stratiform and convective clouds, and at least in regions where $Q_1 < 0$, and in particular in convective regions. Parameter Q_1 can be easily computed from (1)–(5) if either the model is formulated in conserved variables or uses temperature and water vapor or more water species as prognostic variables. Alternatively, the fractional cloudiness can also be determined with the aid of Q_2 . The present approach of fractional cloudiness and cloud condensate in subsaturated regions avoids numerical problems related to the treatment of evaporation and advection of subgrid-scale cloud fields. Finally, the scheme also presents advantages in data assimilation procedures as it provides derivable expressions that consistently link the subgrid-scale cloud field to the large-scale (convectively adjusted) fields of temperature and water vapor.

Acknowledgments. We wish to express our gratitude to P. Mascart for his help in the mesoscale simulations, and to J.-P. Cammas for his help in retrieving satellite data from ECMWF. Also, F. Guichard and M. Tomasini provided the TOGA-COARE forcing data, the ARM forcing was kindly provided by R. L. Cederwall and S. Xie. Finally, the paper resulted from stimulating discussions with A. P. Siebesma, P. Bougeault, J.-I. Yano, and J.-L. Redelsperger. Computer resources have been made available by IDRIS/CNRS, Météo France, and ECMWF.

¹ The corresponding computer code is available as a portable routine in Fortran 90 on <http://www.aero.obs-mip.fr/becp/convect/routinecondens.f90>.

APPENDIX

Definition of Latent and Specific Heats

The specific latent heats of vaporization and sublimation as a function of temperature are defined by

$$L_v(T) = L_v(T_0) + (C_{pv} - C_l)(T - T_0), \quad (\text{A1})$$

$$L_s(T) = L_s(T_0) + (C_{pv} - C_s)(T - T_0), \quad (\text{A2})$$

with $T_0 = 273.16$ K, $L_v(T_0) = 2.5008 \times 10^6$ J kg⁻¹, and $L_s(T_0) = 2.8345 \times 10^6$ J kg⁻¹. The specific heat constants are defined as

$$C_{pv} = 4R_v; \quad C_l = 4.218 \times 10^3 \text{ J kg}^{-1} \text{ K}^{-1};$$

$$C_s = 2.106 \times 10^3 \text{ J kg}^{-1} \text{ K}^{-1}, \quad (\text{A3})$$

with the gas constant for water vapor given as $R_v = 461.525$ J kg⁻¹ K⁻¹. The gas constant and specific heat for dry air are defined as $R_d = 287.06$ J kg⁻¹ K⁻¹ and $C_{pd} = (7/2)R_d$.

REFERENCES

- Bechtold, P., E. Bazile, F. Guichard, P. Mascart, and E. Richard, 2001: A mass flux convection scheme for regional and global models. *Quart. J. Roy. Meteor. Soc.*, **127**, 869–886.
- Bougeault, P., 1981: Modeling the trade-wind cumulus boundary layer. Part I: Testing the ensemble cloud relations against numerical data. *J. Atmos. Sci.*, **38**, 2414–2428.
- , and P. Lacarrère, 1989: Parameterization of orography-induced turbulence in a mesobeta-scale model. *Mon. Wea. Rev.*, **117**, 1872–1890.
- Cederwall, R. T., S. K. Krueger, S. Xie, and J. Yio, 2000: ARM/GCSS Single Column Model (SCM) intercomparison, procedures for case 3: Summer 1997 SCM IOP. Lawrence Livermore National Laboratories Rep. UCRL-ID-141823, 20 pp.
- Chaboureau, J.-P., J.-P. Cammas, P. Mascart, J.-P. Pinty, C. Claud, R. Roca, and J.-J. Morcrette, 2000: Evaluation of a cloud system life-cycle simulated by Meso-NH during FASTEX using METEOSAT radiances and TOVS-3I cloud retrievals. *Quart. J. Roy. Meteor. Soc.*, **126**, 1735–1750.
- , —, —, —, and J.-P. Lafore, 2002: Mesoscale model cloud scheme assessment using satellite observations. *J. Geophys. Res.*, in press.
- Cuijpers, J. W. M., and P. Bechtold, 1995: A simple parameterization of cloud water related variables for use in boundary layer models. *J. Atmos. Sci.*, **52**, 2486–2490.
- Cusack, S., J. M. Edwards, and R. Kershaw, 1999: Estimating the subgrid variance of saturation, and its parameterization for use in a GCM cloud scheme. *Quart. J. Roy. Meteor. Soc.*, **125**, 3057–3076.
- Cuxart, J., P. Bougeault, and J.-L. Redelsperger, 2000: A turbulence scheme allowing for mesoscale and large-eddy simulations. *Quart. J. Roy. Meteor. Soc.*, **126**, 1–30.
- Ebert, E. E., and J. A. Curry, 1992: A parameterization of ice cloud optical properties for climate models. *J. Geophys. Res.*, **97**, 3831–3836.
- Emanuel, K. A., 1994: *Atmospheric Convection*. Oxford University Press, 592 pp.
- Fouquart, Y., 1987: Radiative transfer in climate models. *Physically-Based Modelling and Simulation of Climate and Climatic Changes*, M. E. Schlesinger, Ed., NATO ASI Series, Kluwer Academic, 223–283.
- , and B. Bonnel, 1980: Computations of solar heating of the earth's atmosphere: A new parameterization. *Beitr. Phys. Atmos.*, **53**, 35–62.
- Grabowski, W. W., X. Wu, and M. W. Moncrieff, 1996: Cloud-resolving modeling of tropical cloud systems during phase III of GATE. Part I: Two-dimensional experiments. *J. Atmos. Sci.*, **53**, 3684–3709.
- Guichard, F., J.-L. Redelsperger, and J.-P. Lafore, 2000: Cloud-resolving simulation of convective activity during TOGA-COARE: Sensitivity to external sources of uncertainties. *Quart. J. Roy. Meteor. Soc.*, **126**, 3067–3095.
- Holtzlag, A. A. M., and F. T. M. Nieuwstadt, 1986: Scaling the atmospheric boundary-layer. *Bound.-Layer Meteor.*, **36**, 201–209.
- Kristjánsson, J. E., J. M. Edwards, and D. L. Mitchell, 1999: A new parameterization scheme for the optical properties of ice crystals for use in general circulation models of the atmosphere. *Phys. Chem. Earth*, **24B**, 231–236.
- Lafore, J.-P., and Coauthors, 1998: The Meso-NH Atmospheric Simulation System. Part I: Adiabatic formulation and control simulations. *Ann. Geophys.*, **16**, 90–109.
- Lenderink, G., and P. Siebesma, 2000: Combining the mass flux approach with a statistical cloud scheme. Preprints, *14th Symp. on Boundary Layer and Turbulence*, Aspen, CO, Amer. Meteor. Soc., 66–69.
- Lin, X., and R. H. Johnson, 1996: Kinematic and thermodynamical characteristics of the flow over the western Pacific warm pool during TOGA COARE. *J. Atmos. Sci.*, **53**, 695–715.
- Mellor, G. L., 1977: The Gaussian cloud model relations. *J. Atmos. Sci.*, **34**, 356–358.
- Moncrieff, M., S. K. Krueger, D. Gregory, J. L. Redelsperger, and W.-L. Tao, 1997: GEWEX Cloud System Study (GCSS) Working Group 4: Precipitating convective cloud systems. *Bull. Amer. Meteor. Soc.*, **78**, 831–844.
- Morcrette, J.-J., and Y. Fouquart, 1985: On systematic errors in parameterized calculations of longwave radiation transfer. *Quart. J. Roy. Meteor. Soc.*, **111**, 691–708.
- Smith, R. N. B., 1990: A scheme for predicting layer clouds and their water content in a general circulation model. *Quart. J. Roy. Meteor. Soc.*, **116**, 435–460.
- Sommeria, G., and J. W. Deardorff, 1977: Subgrid-scale condensation in models of nonprecipitating clouds. *J. Atmos. Sci.*, **34**, 344–355.
- Stephens, G. L., 1978: Radiation profiles in extended water clouds. II: Parameterization schemes. *J. Atmos. Sci.*, **35**, 2123–2132.
- Tiedtke, M., 1993: Representation of clouds in large-scale models. *Mon. Wea. Rev.*, **121**, 3040–3061.
- Wu, X., W. D. Hall, W. W. Grabowski, M. W. Moncrieff, W. D. Collins, and J. T. Kiehl, 1999: Long-term behavior of cloud systems in TOGA COARE and their interactions with radiative and surface processes. Part II: effects of ice microphysics and cloud-radiation interaction. *J. Atmos. Sci.*, **56**, 3177–3195.
- Xu, K.-M., and S. K. Krueger, 1991: Evaluation of cloudiness parameterizations using a cumulus ensemble model. *Mon. Wea. Rev.*, **119**, 342–367.
- , and D. A. Randall, 1996: A semiempirical cloudiness parameterization for use in climate models. *J. Atmos. Sci.*, **53**, 3084–3102.
- Zhang, C., and M.-D. Chou, 1999: Variability of water vapor, infrared radiative cooling, and atmospheric instability for deep convection in the equatorial western Pacific. *J. Atmos. Sci.*, **56**, 711–722.
- Zhang, M. H., J. L. Lin, R. T. Cederwall, J. J. Yio, and S. C. Xie, 2001: Objective analysis of ARM IOP data: Method and sensitivity. *Mon. Wea. Rev.*, **129**, 1503–1524.